Journal of Materials Chemistry C

Accepted Manuscript

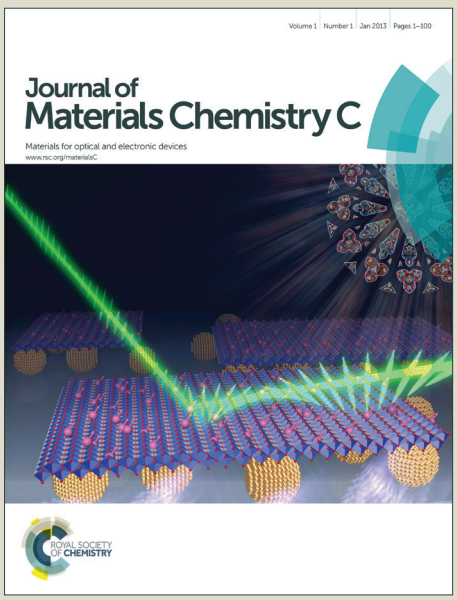

ROYAL SOCIETY OF CHEMISTRY

www.rsc.org/materialsC

Journal Name

RSCPublishing

ARTICLE

Amplified Two-Photon Brightness in Organic Multicomponent Nanoparticles

Cite this: DOI: 10.1039/x0xx00000x

Elisa Campioli,[a] Domna Maria Nikolaidou,[a] Vincent Hugues,[b] Marco Campanini,[c] Lucia Nasi,[c] Mireille Blanchard-Desce*[b,] and Francesca Terenziani*[a]

Received 00th January 2012,
Accepted 00th January 2012

DOI: 10.1039/x0xx00000x

www.rsc.org/

In this paper we show how to easily obtain multicomponent fluorescent organic nanoparticles displaying an excitation energy-transfer cascade between the different molecular components. The use of an optically neutral polymer as dopant helps to increase the colloidal stability of the water suspensions and to slow down luminescence loss over time. In particular, core@shell@shell ternary nanoparticles are designed and investigated, providing a strongly increased luminescence in the red spectral region. The two-photon brightness of the ternary nanoparticles is greatly enhanced with respect to that of the single-component nanoparticles. In addition, these ternary nanoparticles can be two-photon excited over a broad spectral range (from 600 to 1200 nm) inside the biological transparency window. This property, together with the good colloidal stability in water suspension, suggests these fully organic multicomponent nanosystems to be very promising nanoprobes for bioimaging applications.

Introduction

Organic nanoassemblies and, in particular, fluorescent organic nanoparticles (FONs) prepared from small organic molecules have attracted growing attention in the very last years for the simplicity of preparation and their unique optical and optoelectronic properties.[1–9] The most commonly adopted way to prepare organic nanoparticles is the so-called reprecipitation method,[10] consisting in a solvent-exchange process: a concentrated solution of a hydrophobic compound, dissolved in an organic hydrophilic solvent, is rapidly introduced into a large amount of a non-solvent (generally water) under vigorous stirring. The rapid mixing of the two liquids changes the micro-environment of the molecules and induces the precipitation of the compound, which generally forms micro/nanoaggregates or micro/nanocrystals. Nanoparticles with different optical properties can be obtained, such as tunable fluorescence,[11–20] size-dependent luminescence or absorption,[2,21–23] and large nonlinear optical efficiency,[24–31] so that they are expected to serve as novel functional materials in electronics and photonics.

In particular, some recent work focuses on the preparation and characterization of fully organic core@shell nanostructures in water suspension.[7] These types of nanoassemblies are composed by two chromophores chosen as to obtain efficient excitation energy transfer (EET): one dye composes the core of the nanoparticle while the second forms the shell. The EET process takes place mainly at the interface between the core and the shell and, for this reason, the fluorescence of these nanostructures is localized at the core/shell nanointerface, with a consequent shift and amplification of the luminescence with respect to single-component nanoparticles and composite nanoparticles (where the two dyes are randomly mixed to form the nanoassembly).

In this paper we prepare and investigate ternary core@shell@shell nanoassemblies (composed by three different organic chromophores), designed to obtain efficient and directional excitation energy-transfer cascade from the external shell to the inner core. A simple and practical way to improve the colloidal and photophysical stability of the nanoparticles, using an optically neutral polymer, is also proposed. The ternary nanoassemblies are investigated through the two-photon induced fluorescence technique, showing very high two-photon brightness over a wide excitation spectral range inside the biological transparency window, together with an efficient red emission. A huge amplification of the two-photon brightness is observed with respect to single-component nanoparticles, suggesting our ternary nanosystems to be promising candidates as nanoprobes for nonlinear microscopy and bioimaging.

Experimental Section

Synthesis of the chromophores

Chromophores **TW1** and **TW2** were prepared by following the synthetic route described in Ref. 7, while chromophore **TW0** was obtained using the synthesis of Ref. 13. The molecular structures of all the chromophores are reported in Fig. 1.

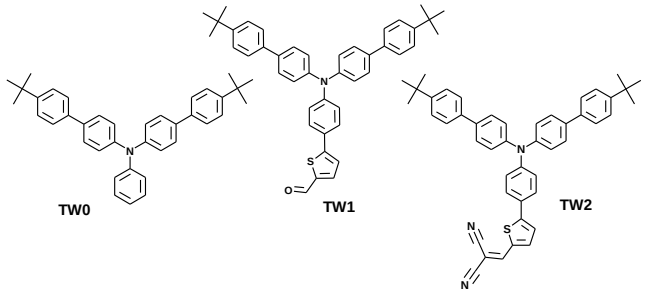

Fig. 1. Molecular structures of the three chromophores.

Preparation of Core@Shell@Shell and Composite Nanoparticles

The preparation of **TW2@TW1@TW0** nanoparticles was carried out using a sequential reprecipitation process, extending the procedure proposed in Ref. 7. In particular, a three-step reprecipitation method was used: first **TW2** FONs were prepared by addition of an aliquot of a concentrated THF solution of **TW2** in a large volume of deionized water under vigorous stirring. In a second step, an aliquot of a concentrated THF solution of **TW1** was added to the aqueous suspension of **TW2** FONs, in order to cover **TW2** FONs with a layer of **TW1**. Finally, an aliquot of a concentrated THF solution of **TW0** was added to the obtained **TW2@TW1** FONs suspension to create an outer layer of dye **TW0**. The final nominal concentration is 1×10^{-5} M for the three different dyes.

A second type of core@shell@shell nanoparticles was prepared using the same starting chromophores but, in this case, a small amount of an optically neutral polymer (polymethylmetacrylate, **PMMA**) was added as a dopant into the nanoparticles. First **PMMA**-doped **TW2** FONs were prepared by reprecipitation in water: **TW2** and **PMMA** solutions in THF were mixed together and a small aliquot of this solution was added to a known large volume of deionized water. Then an aliquot of a THF solution of **TW1** and **PMMA** was added to the obtained **PMMA**-doped **TW2** FONs suspension to obtain **PMMA**-doped **TW2@TW1** FONs. Finally, an aliquot of a THF solution of **TW0** and **PMMA** was added to the binary suspension, to give **TW2@TW1@TW0 PMMA**-doped nanostructures. The final nominal concentration is of 1×10^{-5} M for each one of the three chromophores and 3×10^{-7} M for **PMMA**.

"**Composite**" nanoparticles were obtained via a single-step procedure,[7] by adding a small amount of concentrated THF solution of the three chromophores to a large amount of bi-distilled water under vigorous stirring; "**composite-PMMA**" nanoparticles by adding to water an aliquot of a concentrated THF solution of the three chromophores and **PMMA**. The final nominal concentrations are 1×10^{-5} M for each one of the chromophores and 3×10^{-7} M for **PMMA**.

For comparison, monocomponent **TW0**, **TW1**, **TW2** FONs and **TW0-PMMA**, **TW1-PMMA**, **TW2-PMMA** FONs were prepared using the standard reprecipitation method.

Morphologic and spectroscopic characterization

Conventional transmission electron microscopy (TEM) was carried out using a JEOL 2200FS analytical transmission electron microscopy equipped with in-column energy filter working at 200 kV. To prepare the samples, a droplet of the aqueous suspensions was placed on a carbon grid after the reprecipitation was complete, and the excess liquid was drawn off with paper. Uranyl acetate (2% w/w in water) was used as staining agent. The grids were allowed to dry for 1 day before performing the analysis.

Dynamic light scattering (DLS) was performed using 90Plus Particle Size Analyzer digital autocorrelator (Brookhaven Instruments Corp.) with 635 nm laser at $\theta = 90$ ° and 25 ° C. Data were analyzed using cumulant fit (CMFT) analysis. Zeta-potential analysis was performed using the same 90Plus instrument equipped with BI-PALS option.

UV-vis absorption spectra were recorded on a Perkin Elmer Lambda 650 spectrometer. Steady-state fluorescence spectra and fluorescence decays were carried out on a Horiba Jobin-Yvon Fluoromax-3 spectrofluorometer. Fluorescence decays were measured in a TCSPC (time-correlated single-photon counting) configuration, under excitation from selected nanoLED or laser-diode sources; fluorescence lifetimes were obtained from the reconvolution fit analysis of the decay profiles; the quality of the fits was judged by the reduced χ^2 value ($\chi^2 < 1.1$). The luminescence quantum yields of the suspensions were measured using fluorescein as reference. For comparison, the quantum yields of ternary composite and core@shell@shell nanoparticles and of **TW1** FONs were also measured exciting at 420 nm using a Horiba Jobin-Yvon Fluorolog spectrofluorometer equipped with a center-mount sample holder and an integrating sphere. The two methods gave the same results within 10%.

Two-photon excited fluorescence experiments were performed using a mode-locked Ti:sapphire laser generating 150 fs wide pulses at a 76 MHz repetition rate, with a time-averaged power of several hundreds of mW (Coherent Mira 900 pumped by a 5 W Verdi) in the 700-950 nm spectral range. The fluorescence from the sample was collected in epifluorescence mode. The residual excitation light was removed using a barrier filter. The emission spectra were corrected for the wavelength-dependence of the detection efficiency using correction factors established through the measurement of reference compounds having known fluorescence emission spectra.

Results and Discussion

Design of the multicomponent nanoparticles

The three fluorescent triphenylamine-based push-pull chromophores used to prepare the ternary organic nanoassemblies were selected based on the good colloidal stability of the nanoparticles obtained starting from the single compounds and of their spectroscopic characteristics. In particular, a good overlap is observed between the emission spectrum of **TW0** FONs and the absorption spectrum of **TW1** FONs, and between the fluorescence spectrum of **TW1** FONs and the absorption spectrum of **TW2** FONs (Fig. 2). Therefore, **TW0** can act as energy donor toward **TW1** which, in turn, can act as energy donor toward **TW2**. In core@shell@shell nanoparticles, **TW2** is used to compose the core of the nanoparticle, **TW1** to form the inner shell and **TW0** to compose the external shell (in contact with water). In this way, ternary **TW2@TW1@TW0** nanoassemblies are obtained where efficient cascade EET from the external shell to the inner shell, down to the core is envisaged.

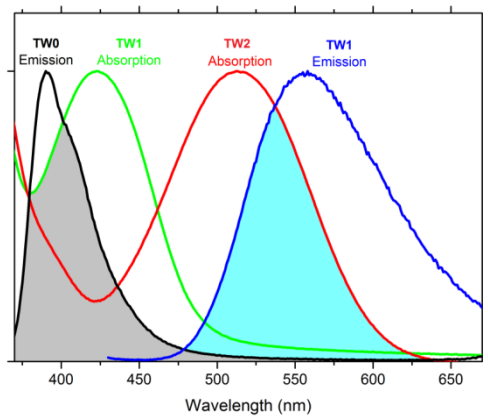

Fig. 2. Spectral overlaps (shadowed areas). Grey area: overlap between the absorption spectrum of **TW1** FONs (green line) and emission spectrum of **TW0** FONs (black line); Blue area: overlap between the absorption spectrum of **TW2** FONs (red line) and the emission spectrum of **TW1** FONs (blue line).

Core@shell@shell **PMMA**-doped nanoparticle were prepared in order to evaluate its role on the colloidal and photophysical stabilization. **PMMA** was chosen for its good transparency in the visible spectral window.

To gain additional information, we also prepared "**composite**" ternary nanoparticles (both **PMMA**-free and **PMMA**-doped), where the three different dyes are randomly mixed inside the nanoassemblies.

Morphology and colloidal stability

The qualitative observation of the suspensions through the naked eyes reveals that no big aggregates are formed either in the freshly prepared suspensions or even after many weeks. In fact, no scattering is observed in absorption and fluorescence spectra, even after some weeks.

The good colloidal stability is confirmed by the Zeta-potential analysis, giving values lower than -30 mV for all the nanoparticles (Table 1).[32] It is interesting to notice that pure **TW0** FONs and nanostructures obtained via the three-step reprecipitation process show very similar Zeta-potentials, sensibly different, for example, from the Zeta-potential value measured for pure **TW2** FONs. This is consistent with the presence of **TW0** at the surface of the nanoparticles prepared via the three-step process.

Most of the nanoparticles were also analyzed through DLS, both over freshly prepared suspensions and on 11-weeks aged ones. Results are collected in Table 1. The DLS (intensity-weighted) effective diameter ranges between 96 and 134 nm, and the polydispersity between 0.14 and 0.24. From these data, the number-weighted mean diameter can be estimated, as also reported in Table 1, ranging from 42 to 60 nm. The effective diameter of the single-component **TW0** and **TW1** nanoparticles and **TW2@TW1@TW0** nanoparticles slightly increases during time (5-10%), while it stays constant for **TW2** nanoparticles and decreases (6%) for **TW0/TW1/TW2** composite nanoparticles. The polydispersity stays constant for **TW1** and **TW2** nanoparticles, while it increases for **TW0** and composite nanoparticles and decreases for **TW2@TW1@TW0** nanoparticles. Consistently, the number-weighted mean diameter decreases for **TW0** and composite nanoparticles, stays roughly constant for **TW1** and **TW2** nanoparticles and significantly increases for core@shell@shell nanoparticles.

Table 1. Colloidal and morphologic characterization of the nanoparticles: Z-potential, DLS (intensity-weighted) effective diameter, polydispersity, DLS number-weighted diameter, TEM mean diameter.

	Z-pot / mV	DLS eff. diameter / nm[a]	Polydispersity	DLS by-number diameter / nm[a]	TEM mean diameter/ nm[a]
TW0	-42±2	134 (141)	0.19 (0.28)	57 (39)	/
TW1	-46±1	133 (144)	0.24 (0.24)	45 (49)	55
TW2	-36±3	96 (96)	0.17 (0.17)	44 (43)	64
Composite	-44±2	118 (111)	0.14 (0.16)	60 (53)	62
TW2@TW1@TW0	-44±2	122 (128)	0.23 (0.18)	42 (57)	42 (56)
TW2@TW1@TW0-PMMA	-40.0±1.5	118 (117)	0.20 (0.21)	47 (44)	41 (48)

[a] For freshly-prepared and, in parentheses, 11-weeks aged nanoparticles.

Journal Name RSCPublishing

ARTICLE

Transmission electron microscopy (TEM) analysis nicely confirms the data obtained via DLS (see Table 1), the mean diameter estimated via TEM being comparable with the number-weighed DLS diameter. TEM analysis points out that the nanoparticles have a spherical shape and confirms a quite high polydispersity. In particular, TEM images of core@shell@shell nanoassemblies (without and with **PMMA**) deposited from freshly prepared suspensions and from 11-weeks-aged suspensions are shown in Fig. 3 (the statistical analysis of their dimension is available as ESI, Fig. S1). The 11-weeks-aged **TW2@TW1@TW0** nanoparticles lacking **PMMA** display a sizable growth of the average diameter compared to the same nanosystems deposited just after preparation (from 42 to 56 nm, also confirmed by DLS). Instead, **TW2@TW1@TW0-PMMA** nanoparticles display only a weak increase of the diameter (41 to 48 nm) after 11 weeks, and also maintain a similar size distribution. This is a nice evidence of the effect of further stabilization due to the presence of **PMMA**.

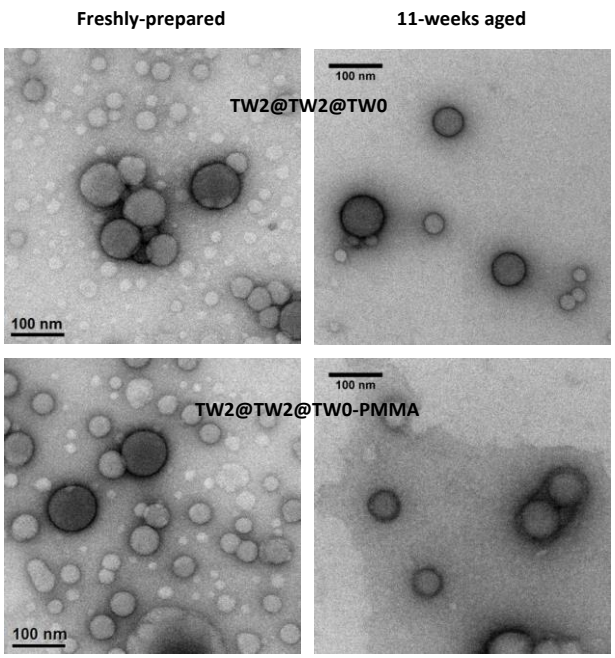

Fig. 3. TEM images of freshly prepared (left) and 11-weeks aged (right) core@shell@shell nanoparticles. Top: **TW2@TW1@TW0** nanoparticles. Bottom: **TW2@TW1@TW0-PMMA** nanoparticles.

Spectroscopic characterization

The main spectroscopic properties of the investigated nanoparticles suspensions are summarized in Table 2. Absorption spectra of the undoped nanoparticles suspensions are shown in Fig. 4 (see Fig. S2, ESI, for absorption spectra of the **PMMA**-doped nanoparticles). The absorption spectra of the ternary nanosystems show three major bands due to the superposition of the absorption spectra of the three dyes.

Fluorescence spectra of the undoped nanoparticles suspensions are reported in Fig. 5 (see Fig. S3, ESI, for fluorescence spectra of **PMMA**-doped nanoparticles). When the core@shell@shell nanoparticles (without or with **PMMA**) are excited at 340 nm (Fig. 5a and S3a), where all of the three compounds absorb, the emissions of **TW0** and **TW1** are strongly quenched, while the emission of **TW2** in the red spectral region is strongly enhanced. A similar behavior is observed in composite nanoparticles, with a complete quenching of the emissions from **TW0** and **TW1** and an enhancement of the fluorescence signal from **TW2**. It is interesting to notice that the fluorescence of core@shell@shell nanoparticles is sizably blue-shifted compared to the emission of the acceptor (**TW2**) nanoparticles and of composite nanoparticles as well.

Table 2. Spectroscopic properties of the freshly-prepared nanoparticles suspensions. The quantum yields were obtained by exciting at different wavelengths: 340 nm for **TW0** FONs, **TW2@TW1@TW0** FONs and composite FONs; 420 nm for **TW1** FONs; 520 nm for **TW2** FONs. No significant differences in quantum yields are detected when ternary systems are excited at 340 nm or 420 nm.

	λ_{abs}^{max} / nm	λ_{em}^{max} / nm[a]	Φ
TW0	331	390; / ; /	0.08
TW1	342; 422	552; 552; /	0.07
TW2	340; 515	697; 697; 697	0.06
Composite	336; 424; 524	675; 675; 675	0.15
TW2@TW1@TW0	338; 423; 514	623; 625; 692	0.20
TW0-PMMA	331	391; / ; /	0.13
TW1-PMMA	341; 422	546; 546; /	0.09
TW2-PMMA	340; 514	700; 700; 700	0.07
Composite-PMMA	338; 426; 521	673; 673; 675	0.14
TW2@TW1@TW0-PMMA	338; 421;516	652; 648; 687	0.15

[a] For excitation at 340; 420; 520 nm, respectively.

When **TW2@TW1@TW0** nanoparticles are excited at 420 nm (Fig. 5b and S3b), where only **TW1** has a sizable absorption, the emission of **TW1** is strongly (but not completely) quenched and the luminescence spectrum (from **TW2** acceptor) is very similar to what observed for excitation at 340 nm. From the decrease of the emission intensity of the donor (**TW1**) with respect to the single-component nanoparticles, the efficiency of the EET process from **TW1** to

TW2 in the core@shell@shell nanoparticles can be estimated to 90%. Composite **TW0/TW1/TW2** nanoparticles excited at 420 nm instead show a complete quenching of the **TW1** emission and an enhanced emission from the **TW2** acceptor, similar to what observed for excitation at 340 nm.

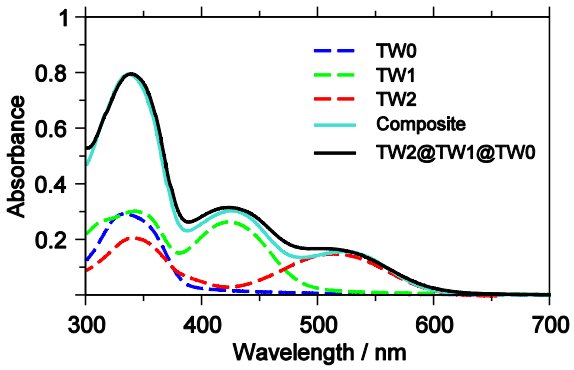

Fig. 4. Absorption spectra of the undoped nanoparticles suspension.

When the ternary nanoassemblies are excited at 520 nm (Fig. 5c and S3c), where **TW0** and **TW1** do not absorb, only **TW2** is selectively and directly excited and is hence responsible for the luminescence signal. It can be noticed that, in this case, core@shell@shell nanoparticles basically recover the same emission spectrum (in terms of position and intensity) as **TW2** FONs, while the fluorescence spectrum of composite structures is slightly blue-shifted compared to the spectrum of pure **TW2** FONs. A very similar behavior had been observed in binary **TW2@TW1** and composite **TW2/TW1** nanoparticles.[7]

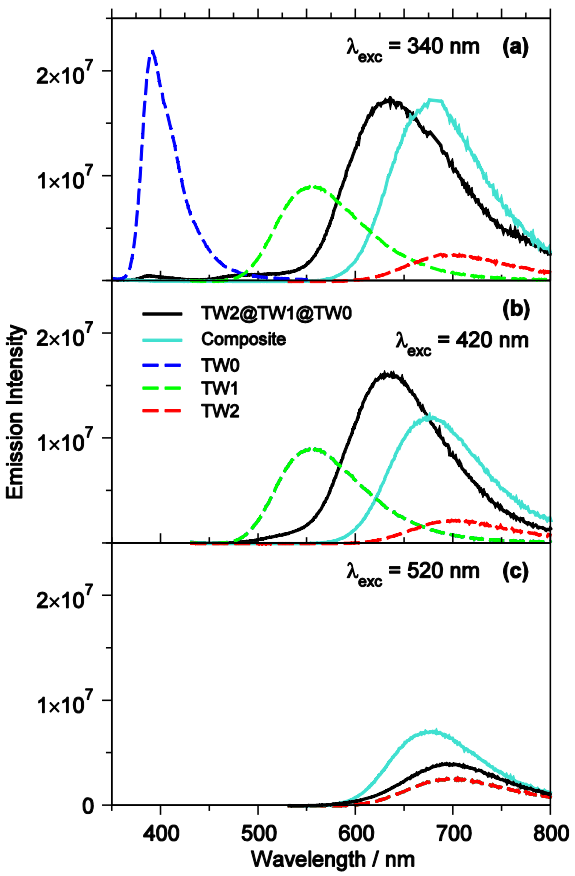

Fig. 5. Fluorescence emission spectra of the freshly-prepared undoped nanoparticles suspensions for different excitation wavelengths.

The fluorescence characteristics of our nanostructures are strongly affected by the organization of the chromophores inside the nanoparticles. In the layered core@shell@shell structures an EET cascade takes place from the external to the inner shell and finally to the core. As discussed in Ref. [7], the luminescence from the core after EET is localized at the core/shell nanointerface, where the EET probability is maximized. The blue-shifted emission is related to the difference in environment as compared to pure acceptor nanoparticles and to the direct acceptor excitation (at 520 nm) in the core@shell@shell nanoparticles. The situation is different for composite nanostructures: in this case the chromophores are supposedly randomly distributed inside the nanoparticles, so that all of the acceptor molecules statistically have the same environment; as a consequence, the emission from the acceptor is independent of the excitation wavelength, i.e. it is the same if the acceptor is directly excited or if it becomes excited via EET.

Fluorescence excitation profiles (Fig. 6) confirm this interpretation. In fact, the excitation profile of composite nanoparticles is independent of the emission wavelength (Fig. 6b), while the excitation spectrum of core@shell@shell nanoparticles strongly depends on the emission wavelength (Fig. 6a). In particular, when detecting at long wavelength (700 nm), the excitation profile has a contribution from all of the

three chromophores that compose the nanoparticles, while emission at shorter wavelength (625 nm) is mainly originated by direct excitation of **TW0** and **TW1** chromophores in the two shells (and subsequent EET to the core **TW2** chromophores at the core/shell nanointerface).

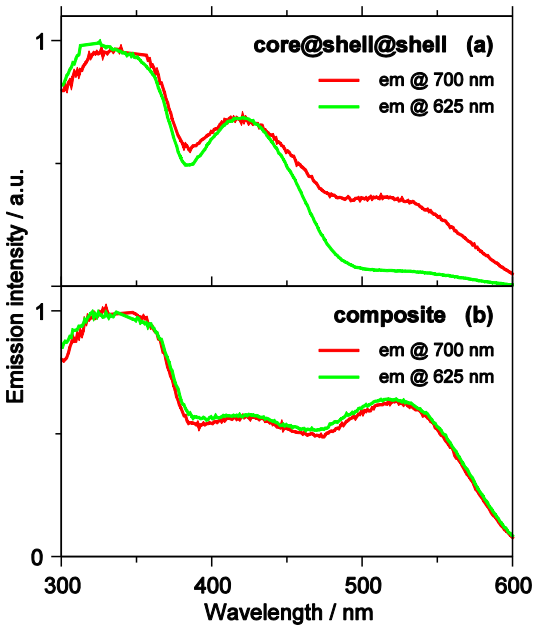

Fig. 6. Normalized fluorescence excitation profiles of **TW2@TW1@TW0** nanoparticles (a) and composite ternary nanoparticles (b) for detection at different emission wavelengths.

To fully characterize the excitation energy transfer process, we also investigated the photoluminescence dynamics of all the prepared nanosystems (Table S1 and S2, ESI). The fluorescence decays are found to be three-exponential for all nanoparticles, whatever the excitation wavelength.

For excitation wavelength at 340 nm (Table S1, ESI), the fluorescence decays are measured at the three maximum-emission wavelengths of the three compounds. When detecting at 620 nm (corresponding to the emission of the core **TW2**), an about threefold increase of the energy-acceptor lifetime is obtained for core@shell@shell nanostructures, while an about twofold increase is found in composite nanostructures. Instead, if the fluorescence decays are measured at 400 and 525 nm (the emitting regions of **TW0** and **TW1**, respectively) a major shortening of the fluorescence lifetimes is recorded for the ternary nanoassemblies. The marked shortening of the donors luminescence lifetimes and the lengthening of the acceptor luminescence lifetime in these nanostructures provide nice confirmation of the efficient **TW0→TW1→TW2** energy-transfer cascade.

The fluorescence decays were also measured at 620 nm for excitation wavelength at 405 nm, corresponding to an almost selective excitation of **TW1** in the inner shell (Table S2, ESI): the EET process from **TW1** to **TW2** is clearly confirmed by the approximately threefold and twofold lengthening of the energy-acceptor lifetimes for core@shell@shell and composite nanosystems, respectively.

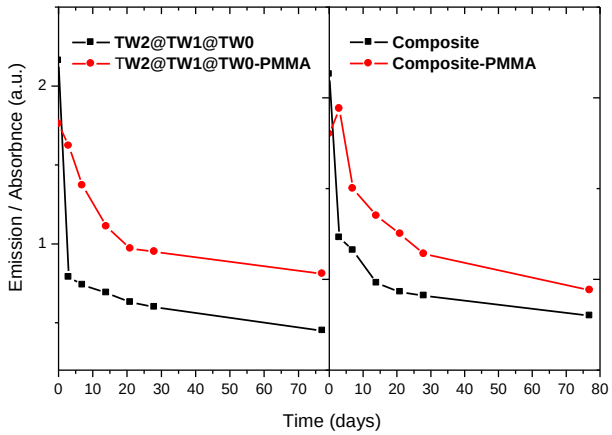

Fig. 7. Temporal evolution of the ratio between the intensity of emission (at the maximum) and the absorbance (at the excitation wavelength) of core@shell@shell and composite nanoparticles, without (black) and with (red) PMMA.

The absorption and fluorescence spectra of core@shell@shell and composite nanostructures (without and with **PMMA**) were monitored during time, for up to 11 weeks (Fig. S4 and Fig. S5, ESI). The absorption spectra are quite stable during time: only a slight progressive growth of the three bands is observed, which can safely be ascribed to a small variation of the concentration, due to a partial evaporation of water. The emission spectrum of core@shell@shell nanoparticles without **PMMA** dramatically decreases after three days, then the decrease becomes much slower and no significant change is detected any more after 11 weeks. Instead, the emission spectrum of **PMMA**-doped core@shell@shell nanoassemblies has a much less pronounced initial decrease, but a smooth decrease is anyhow detected for a few weeks. A similar behavior is observed for composite nanoparticles. The ratio between the emission maximum and the absorbance at the excitation wavelength (proportional to the quantum yield) is reported in Fig. 7 as a function of time. This ratio (and hence the quantum yield) decreases both for undoped and doped nanoassemblies, but the slope is steeper in undoped systems and their quantum yield stays always lower than for **PMMA**-doped systems. As there is no significant variation of the absorption spectra (meaning that no massive inter-nanoparticles aggregation takes place) the intensity variation of the emission spectra can be mainly ascribed to a slow rearrangement of molecules inside the nanoparticles, such as anti-parallel orientation of the dipolar chromophores leading to reduced radiative decay rates and favoring competing non-radiative decay processes (such as electron transfer). Apparently, the presence of **PMMA** plays a role in reducing such effects by reducing interactions between chromophores and slowing down their rearrangement within the nanoparticles.

Two-photon excited fluorescence

The ternary nanosystems and the corresponding monocomponent nanoparticles were investigated with the two-photon excited fluorescence (TPEF) technique. Briefly, the experimental set-up allows for the recording of corrected fluorescence emission spectra under multiphoton excitation at variable excitation powers and wavelengths. Whatever the excitation wavelength, extremely weak TPEF signals were detected from monocomponent FONs. Even when exciting at 840 nm, i.e. twice the wavelength of maximum one-photon absorption of **TW1**, only a very weak TPEF signal is detected for **TW1** FONs (Fig. 8). No significant TPEF signal could either be detected from **TW2** nanoparticles, even when two-photon pumping at 1040 nm, i.e. twice the one-photon maximum absorption wavelength of **TW2** (Fig. S6, ESI).

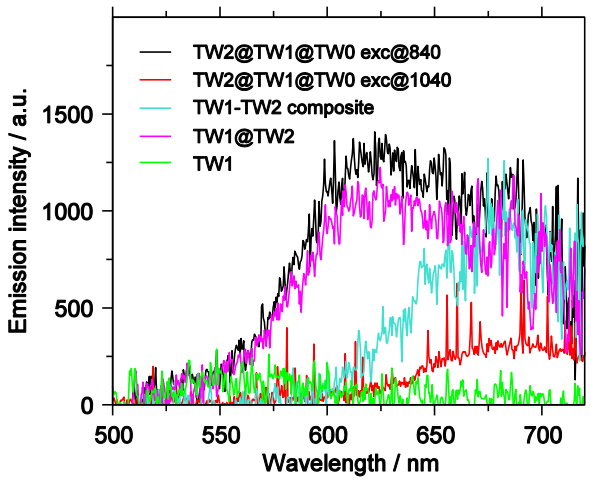

Fig. 8. Two-photon excited fluorescence spectra, for two-photon excitation at 840 nm, of **TW2@TW1@TW0** nanoparticles (black line), binary **TW2@TW1** nanoparticles (magenta line), binary **TW1/TW2** composite nanoparticles (turquoise line) and **TW1** nanoparticles (green line). The two-photon excited fluorescence spectrum of **TW2@TW1@TW0** nanoparticles is also reported for two-photon excitation at 1040 nm (red line).

Multicomponent nanoparticles, instead, show well detectable TPEF spectra (Fig. 8) that nicely correspond to those obtained with standard one-photon excitation (Fig. S7, ESI). In particular, when pumping at 840 nm, where **TW1** is almost selectively two-photon excited (since at 420 nm the linear absorption of **TW0** and **TW2** is very low), the multicomponent nanoparticles suspensions show a dramatic increase of the two-photon induced fluorescence signal. The fluorescence signal clearly arises from **TW2** molecules that get indirectly excited via excitation energy transfer from **TW1**, as already observed in the case of one-photon excitation. The same trend is observed as in one-photon induced fluorescence spectra, i.e. the TPEF signal from core@shell@shell nanoparticles is blue-shifted with respect to the TPEF signal from composite nanoparticles. A well detectable TPEF signal is also measured for core@shell@shell nanoparticles when two-photon excited at 1040 nm, i.e. when directly exciting **TW2** molecules in the core.

The amplification of the TPEF signal in ternary nanoparticles cannot be simply ascribed to the increased luminescence quantum yield (Φ) of composite and core@shell@shell nanoparticles with respect to the monocomponent nanoparticles. In fact, the quantum yield gain accounts only for an about threefold amplification (see Table 2), while the observed TPEF enhancement amounts to ~ 12 for ternary nanoparticles excited at 840 nm. The intensity of the TPEF signal is proportional to the $\sigma_2\Phi$ product, where σ_2 is the two-photon absorption cross section. Since in the case of two-photon excitation at 840 nm only **TW1** sizably absorbs, in our case the intensity of the TPEF signal is proportional to the two-photon absorption cross section of **TW1** at 840 nm. Therefore, our results demonstrate that the σ_2 of **TW1** is strongly amplified, by a factor of about 4, in the ternary nanosystems with respect to the monocomponent nanoparticles. Similarly, the TPA cross section of **TW2** is also strongly amplified in core@shell@shell nanoparticles with respect to monocomponent nanoparticles, but the amplification factor cannot be estimated, as the TPEF signal from pure **TW2** nanoparticles is too weak to be quantified.

The estimated molecular TPA cross section for **TW1** nanoparticles is 35 GM at 840 nm. The estimation of the TPA cross section of core@shell@shell nanoparticles is smooth for excitation at wavelengths longer than 1000 nm, i.e. when only **TW2** gets two-photon excited and the TPEF signal is simply due to the emission of the directly excited **TW2** molecules. For core@shell@shell nanoparticles we obtain a TPA cross section of about 80 GM at 1040 nm. On the other hand, the estimation of the TPA cross section of multicomponent nanoparticles is not straightforward when EET occurs. When exciting at wavelengths shorter than 1000 nm, also **TW1** starts two-photon absorbing (below 800 nm also **TW0** would get two-photon excited) but emission still stems from **TW2** molecules that get excited via EET from **TW1** (or **TW0**). Therefore, in order to estimate the correct TPA cross section at wavelengths shorter that 1000 nm, the precise energy-transfer quantum yield is needed. Assuming a 100% yield of the EET process, a nominal TPA cross section amounting to 120 GM at 840 nm is estimated for **TW1** in the core@shell@shell nanoparticles. But this value is the lower-limit threshold for σ_2, that has to be corrected for the EET quantum yield (estimated to amount to 0.9 from single-photon excitation at 420 nm), leading to a final value of 133 GM. This analysis confirms that the amplification factor of the TPA cross section of **TW1** in core@shell@shell nanoparticles with respect to **TW1** single-component nanoparticles amounts to about 4 (at 840 nm).

The source of the remarkable amplification of the two-photon absorption cross section of multicomponent nanoparticles can be related to the different environment experienced by the chromophores with respect to single-component nanoparticles, and to local fields developing inside the ternary nanostructures at the boundary regions between the different molecular components. Indeed two-photon absorption

has been found earlier to be extremely sensitive to weak and short-range electrostatic effects.[33]

The molecular two-photon brightness ($\sigma_2\Phi$) of our **TW2@TW1@TW0** nanoparticles amounts to 27 GM at 840 nm (which is well suitable for bioimaging) versus 2 GM for **TW1** single-component nanoparticles. It is worth estimating the two-photon brightness per nanoparticle, by means of the mean diameter obtained via DLS and a tentative density of 1.35 g/cm^3 (based on the crystal density of similar compounds):[30] we obtain 1.4×10^5 GM for **TW1** nanoparticles, and 1.2×10^6 GM for **TW2@TW1@TW0** nanoparticles. These correspond to a two-photon brightness per unit nanoparticle-volume of 3 GM/nm^3 for **TW1** nanoparticles, and 32 GM/nm^3 for **TW2@TW1@TW0** nanoparticles at 840 nm. This last value is much higher than what is reported for other nanoaggregates[13] or fluorescently doped mesoporous nanoparticles,[34] and even better than CdSe-ZnS water-soluble quantum dots.[35]

Conclusions

In this article we reported the preparation, characterization and spectroscopic time evolution of ternary organic nanoassemblies composed by triphenylamine-based chromophores (named **TW0**, **TW1** and **TW2**). From a structural point of view, two kinds of nanoparticles have been prepared through the reprecipitation method: in the first type, called core@shell@shell, the molecules are arranged in a layered nanostructure composed of an inner core (**TW2**), a middle shell (**TW1**) and an external shell (**TW0**); in the second type, called composite, the three dyes are randomly mixed together to form the nanoparticles. Furthermore, **PMMA**-doped nanoparticles have been prepared to evaluate the possible role of the optically neutral polymer in the colloidal and spectroscopic stabilization of our organic nanostructures.

The good colloidal stability of our nanosystems has been demonstrated through different experimental tests, such as absorption and fluorescence spectra, Zeta-potential, DLS and TEM analysis. The relatively good colloidal stability appears to be further improved by polymer doping. The specific PMMA doping could be of particular interest for materials applications, while more biocompatible polymeric additives or suitable molecular engineering of the dipolar chromophoric subunits of the nanoparticles could be preferred for bioimaging applications.[3,11]

The absorption and fluorescence spectra of all the nanoparticles have been monitored during 11 weeks: while no significant variation of the absorption spectra is observed, a decrease of the emission spectra is detected. This process can be ascribed to the slow rearrangement of molecules inside the nanoparticles. The presence of **PMMA** reduces these effects most probably by weakening intermolecular interactions between chromophoric subunits and slowing down the rearrangement leading to deleterious mutual orientation (i.e. anti-parallel association of dipolar chromophoric subunits) and possibly reducing chromophore-water interactions.

The prepared ternary nanoparticles show a very efficient EET cascade between the three molecular components, with a strong enhancement of the acceptor emission with respect to monocomponent nanoparticles. The luminescence behavior of core@shell@shell and composite nanoparticles is different because of the different organization of the chromophores in the two types of ternary nanostructures. In the core@shell@shell systems, the cascade EET process mainly excites the acceptor molecules in the core lying at the core/shell interface, producing a different luminescence signal than promoted by direct excitation of **TW2** molecules in the core. This behavior is not observed in composite nanoassemblies, where chromophores are randomly distributed and the luminescence from the acceptor is the same independently of the excitation process (direct excitation or EET).

The enhanced luminescence observed in ternary nanoparticles upon standard one-photon excitation prompted us to investigate their two-photon excited fluorescence (TPEF) properties. Strikingly, we obtained a more than tenfold increase of the two-photon induced fluorescence signal with respect to single-component nanoparticles (the molecular two-photon brightness at 840 nm amounts to 27 GM for core@shell@shell nanoparticles, versus barely 2 GM for pure **TW1** nanoparticles). The enhancement of the two-photon brightness cannot be solely ascribed to the increased luminescence efficiency, but is also related to a marked amplification of the TPA cross section of the donor molecules in the ternary nanoparticles. In fact the TPA cross section of **TW1** in core@shell@shell nanoparticles amounts to 133 GM (at 840 nm), i.e. *4 times higher* with respect to **TW1** single-component nanoparticles.

Therefore, we demonstrated that the indirect excitation of the acceptor chromophores via EET from antenna donor molecules in the same nanoparticle is a very interesting root to improve the two-photon brightness, achieving very interesting results, comparable or even better with respect, for example, to water-soluble quantum dots. Moreover, the exploitation of EET from one of more donor species to obtain emission from the sink fluorophore widens the spectral range of excitation, covering a large part of the biological transparency window (from 600 to 1200 nm), still getting an orange-red emission. While a huge amplification of the two-photon brightness is observed in both types of ternary nanostructures, core@shell@shell nanoparticles have the advantage of higher luminescence quantum yield and a directional EET cascade (from the external shell to the inner one to the core, in our case). This last characteristic not only allows to localize the emission in a sub-nanoparticle volume, but also to drive the energy flow towards a specific core/shell nanointerface that acts as a nano-heterojunction.

Acknowledgements

EC, MBD and FT acknowledge the Italo-French University for funding through the Vinci Program. FT thanks "Fondazione Cariparma" for financial support and MIUR (Italian Ministry of

University and Research) for funding through the Project FIRB-Futuro in Ricerca RBFR10Y5VW. MBD gratefully acknowledges the "Conseil Régional d'Aquitaine" for financial support through the "Chaire d'Excellence" grant, and CNRS for a fellowship to VH. The work was partially supported by European Union through FP7-Marie Curie Actions: ITN Nano2Fun Grant Agreement No. 607721. Giancarlo Salviati (IMEM CNR, Parma) and Prof. Antonio Deriu (Parma University) are acknowledged for making the TEM and DLS/Zeta-potential facilities available, respectively.

Notes and references

[a] Dipartimento di Chimica, Università di Parma & INSTM UdR Parma, Parco Area delle Scienze 17/a, 43124 Parma, Italy. Tel: +39 0521905453; E-mail: francesca.terenziani@unipr.it
[b] Univ. Bordeaux, Institut des Sciences Moléculaires (CNRS UMR 5255), 351 Cours de la Libération, 33405 Talence, France. Tel: +33 (0)540006732; E-mail: mireille.blanchard-desce@u-bordeaux.fr
[c] CNR-IMEM, Parco Area delle Scienze 37/a, 43124 Parma, Italy.

† Electronic Supplementary Information (ESI) available: Distribution analysis by TEM; Absorption and emission spectra of the PMMA-doped nanoparticles suspensions; temporal evolution of the absorption and fluorescence spectra of core@shell@shell nanoparticles; two-photon excited fluorescence spectra vs one-photon excited fluorescence spectra; fluorescence lifetimes. See DOI: 10.1039/b000000x/

1. T. Asahi, T. Sugiyama, and H. Masuhara, *Acc. Chem. Res.*, 2008, **41**, 1790–1798.
2. H. Fu and J. Yao, *J. Am. Chem. Soc.*, 2001, **123**, 1434–1439.
3. E. Genin, Z. Gao, J. a Varela, J. Daniel, T. Bsaibess, I. Gosse, L. Groc, L. Cognet, and M. Blanchard-Desce, *Adv. Mater.*, 2014, **26**, 2258–2261.
4. O. H. Ho, *Angew. Chem. Int. Ed.*, 2001, **40**, 4330–4361.
5. R. Jagannathan, G. Irvin, T. Blanton, and S. Jagannathan, *Adv. Funct. Mater.*, 2006, **16**, 747–753.
6. T. O. McDonald, P. Martin, J. P. Patterson, D. Smith, M. Giardiello, M. Marcello, V. See, R. K. O'Reilly, A. Owen, and S. Rannard, *Adv. Funct. Mater.*, 2012, **22**, 2469–2478.
7. E. Campioli, C. Rouxel, M. Campanini, L. Nasi, M. Blanchard-Desce, and F. Terenziani, *Small*, 2013, **9**, 1982–1988.
8. A. Patra, C. G. Chandaluri, and T. P. Radhakrishnan, *Nanoscale*, 2012, **4**, 343–359.
9. K. E. Snell, J.-Y. Mevellec, B. Humbert, F. Lagugné-Labarthet, and E. Ishow, *ACS Appl. Mater. Interfaces*, 2015, **7**, 1932–1942.
10. H. Kasai, H. S. Nalwa, H. Oikawa, S. Okada, H. Matsuda, N. Minami, A. Kakuta, K. Ono, A. Mukoh, and H. Nakanishi, *Jpn. J. Appl. Phys.*, 1992, **31**, L1132–L1134.
11. K. Amro, J. Daniel, G. Clermont, T. Bsaibess, M. Pucheault, E. Genin, M. Vaultier, and M. Blanchard-Desce, *Tetrahedron*, 2014, **70**, 1903–1909.
12. J. Chen, P. Zhang, G. Fang, P. Yi, F. Zeng, and S. Wu, *J. Phys. Chem. B*, 2012, **116**, 4354–4362.
13. E. Ishow, A. Brosseau, G. Clavier, K. Nakatani, P. Tauc, C. Fiorini-Debuisschert, S. Neveu, O. Sandre, and A. Léaustic, *Chem. Mater.*, 2008, **20**, 6597–6599.
14. T. Ishi-i, K. Ikeda, Y. Kichise, and M. Ogawa, *Chem. Asian J.*, 2012, **7**, 1553–1557.
15. X. Li, Y. Qian, S. Wang, S. Li, and G. Yang, *J. Phys. Chem. C*, 2009, **113**, 3862–3868.
16. a.-D. Peng, D.-B. Xiao, Y. Ma, W.-S. Yang, and J.-N. Yao, *Adv. Mater.*, 2005, **17**, 2070–2073.
17. C. Wu, Y. Zheng, C. Szymanski, and J. McNeill, *J. Phys. Chem. C*, 2008, **112**, 1772–1781.
18. C. Zhang, Y. S. Zhao, and J. Yao, *New J. Chem.*, 2011, **35**, 973–978.
19. O. Simalou, R. Lu, P. Xue, P. Gong, and T. Zhang, *European J. Org. Chem.*, 2014, **2014**, 2907–2916.
20. A. Jana, K. T. Nguyen, X. Li, P. Zhu, N. S. Tan, H. Agren, and Y. Zhao, *ACS Nano*, 2014, **8**, 5939–5952.
21. A. J. Gesquiere, T. Uwada, T. Asahi, H. Masuhara, and P. F. Barbara, *Nano Lett.*, 2005, **5**, 1321–1325.
22. H. Fu, X. Ji, X. Zhang, S. Wu, and J. Yao, *J. Colloid Interface Sci.*, 1999, **180**, 177–180.
23. T. Funada, T. Hirose, N. Tamai, and H. Yao, *Phys. Chem. Chem. Phys.*, 2015, **17**, 11006–11013.
24. M.-C. Hsieh, C.-H. Chien, C.-C. Chang, and T.-C. Chang, *J. Mater. Chem. B*, 2013, **1**, 2350–2357.
25. Z. Xu, Q. Liao, Y. Wu, W. Ren, W. Li, L. Liu, S. Wang, Z. Gu, H. Zhang, and H. Fu, *J. Mater. Chem.*, 2012, **22**, 17737–17743.
26. Y. Jiang, Y. Wang, J. Hua, J. Tang, B. Li, S. Qian, and H. Tian, *Chem. Commun.*, 2010, **46**, 4689–4691.
27. S. B. Noh, R. H. Kim, W. J. Kim, S. Kim, K.-S. Lee, N. S. Cho, H.-K. Shim, H. E. Pudavar, and P. N. Prasad, *J. Mater. Chem.*, 2010, **20**, 7422–7429.
28. J. S. Park, R. H. Kim, N. S. Cho, H.-K. Shim, and K.-S. Lee, *J. Nanosci. Nanotechnol.*, 2008, **8**, 4793–4796.
29. S. Kim, Q. Zheng, G. S. He, D. J. Bharali, H. E. Pudavar, a. Baev, and P. N. Prasad, *Adv. Funct. Mater.*, 2006, **16**, 2317–2323.
30. V. Parthasarathy, S. Fery-Forgues, E. Campioli, G. Recher, F. Terenziani, and M. Blanchard-Desce, *Small*, 2011, **7**, 3219–3229.
31. X. Shi, Z. Xu, Q. Liao, Y. Wu, Z. Gu, R. Zheng, and H. Fu, *Dye. Pigment.*, 2015, **115**, 211–217.
32. R. J. Hunter, *Zeta Potential in Colloid Science: Principles and Applications*, Academic Press, London, 1981.
33. C. Rouxel, M. Charlot, O. Mongin, T. R. Krishna, A. M. Caminade, J. P. Majoral, and M. Blanchard-Desce, *Chem. Eur. J.*, 2012, **18**, 16450–16462.
34. R. O. Al-Kaysi, A. M. Müller, T.-S. Ahn, S. Lee, and C. J. Bardeen, *Langmuir*, 2005, **21**, 7990–7994.
35. D. R. Larson, W. R. Zipfel, R. M. Williams, S. W. Clark, M. P. Bruchez, F. W. Wise, and W. W. Webb, *Science*, 2003, **300**, 1434–1436.